

Full Length Research Paper

Flexural behavior of RC beams strengthened with composite beam

Ki Nam Hong^{1*}, Bong Ho Lee², Jong Hoe Kim³, Il Young Jang³ and Sang Hoon Han¹

¹Department of Civil Engineering, Chungbuk National University, San 12, Gaesin-dong, Cheongju-si, Chungbuk-do, 361-763, South Korea.

²Nexcoms Company Limited, 929-1, Toplip-dong, Yoosung-Ku, Deajong-si, South Korea.

³Department of Civil Engineering, Kumoh National Institute of Technology, Sanho-ro 77, Gumi-si, Gyeongbuk-do, 730-701, South Korea.

Accepted 11 April, 2011

This paper presents the results of an experimental and analytical study conducted to assess the strengthening efficiency of a composite beam developed with the goal of simultaneously increasing the flexural stiffness and flexural strength of aging RC structures. A 4-point flexural test was performed on 12 RC beams that were 4.4 m in length. As test variables, the strengthening material (Type-A, B), epoxy type (organic epoxy, and inorganic epoxy), power pin interval (100, 200 mm), and cross-sectional size of the specimen (600 × 200 mm, 300 × 450 mm) were considered. Bond failure occurred in the specimen using inorganic epoxy, whereas in all of the other strengthened specimens, failure occurred as the result of composite beam fracture. The power pin interval and strengthening material type appeared to have very small impacts on the flexural strength of a strengthened RC beam, whereas the epoxy type and cross-sectional size of the specimen showed large impacts. In addition, the analysis model proposed for predicting the flexural behavior of a composite beam-strengthened RC beam was shown to provide relatively accurate predictions for the load-displacement behavior of a specimen in both the elastic and plastic sections.

Key words: Flexural test, composite beam, strengthening material, analysis model.

INTRODUCTION

When an existing RC (reinforced concrete) structure ages and can no longer bear its design load, the structure must be strengthened. At such a point, a suitable material and strengthening method should be selected by taking into account the conditions of the structure and its surroundings. Steel and FRP (fiber reinforced polymer) are the most commonly used strengthening materials for RC structures. In particular, FRP is widely used in the field of strengthening because it has large advantages in terms of its strength, light weight, and corrosion resistance. However, if adequate bond strength between the FRP and structure is not secured, the optimal efficiency of the FRP material cannot be achieved and premature failure can occur (Chen and Tang, 2001; Ehsani

et al., 1993; Seracino et al., 2007; Teng et al., 2003). Such a premature failure is a sudden brittle failure and is not undesirable. Therefore, research has been performed in recent years on making optimal use of the material efficiency of FRP and simultaneously preventing premature failure.

Based on a conjecture that the debonding failure of an FRP plate-strengthened RC beam is affected by the shear span-to-depth ratio, Garden et al. (1997) performed a flexural test that took into account the shear span-to-depth ratio as a test variable. From the test study results, it was reported that the possibility of debonding failure is high for specimens produced with a small shear span-to-depth ratio because of the large shear stress occurring at the end of the FRP plate. As a means of solving the problem of a reduction in the strengthening efficiency of an FRP-strengthened structure because of premature failure, Lamanna et al. (2001) developed powder actuated

*Corresponding author. E-mail: hong@chungbuk.ac.kr.

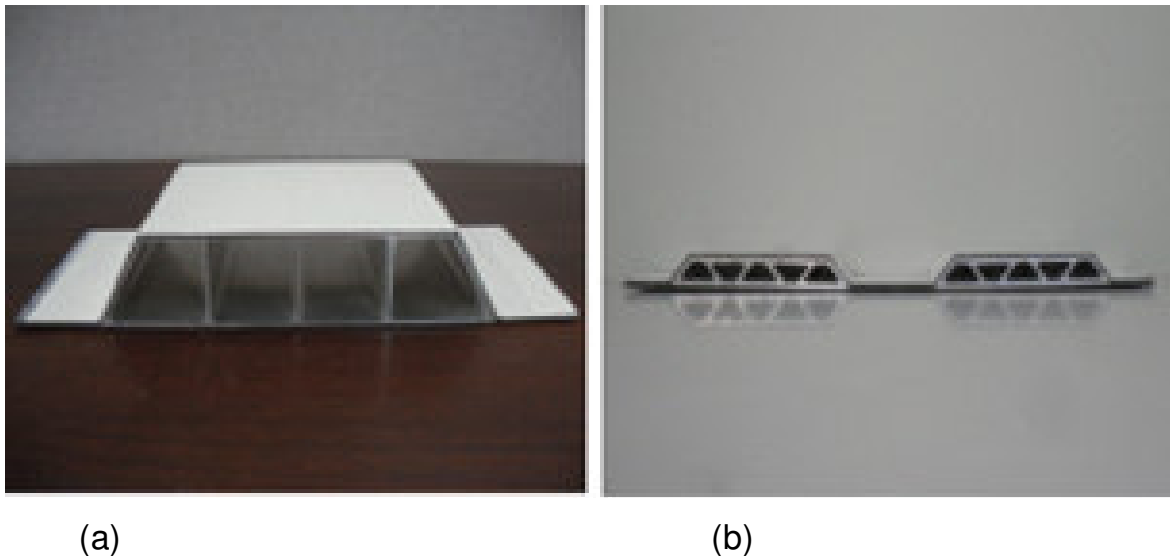


Figure 1. Composite-beam: (a) Type-A (b) Type-B.

fastening systems to attach the FRP strips to the concrete surface and performed an efficiency assessment test. This test confirmed that, although the maximum load of the FRP composite-strengthened specimen was reduced by 30 to 35% compared to an externally attached FRP specimen, the ductility was greatly increased. El-Hacha et al. (2004) performed a flexural test on 8 T-beams to analyze the efficiency of the NSM (near surface mounted) method developed for preventing debonding failure. This test revealed that the strengthening efficiency of specimens strengthened using the NSM method was outstanding because no FRP debonding occurred, and therefore the NSM method could replace the external attachment method. Wu et al. (2006) performed a flexural test on specimens with a CFRP sheet attached to the tensile zone and a GFRP sheet wrapped around the concrete member. Based on the test results, it was reported that the specimens strengthened using the method proposed by Wu et al. showed flexural resistance by the CFRP sheet and slippage prevention by the GFRP sheet and consequently displayed large increases in flexural stiffness and flexural strength. Woo et al. (2006) carried out a flexural test on specimens strengthened with CFRP plates strained by 0.0 to 0.8% and bonded to the tensile zone of the RC beam. In this test, all of the specimens with the CFRP plates anchored on both ends were shown to reach failure because of CFRP fracture regardless of the prestressing level, whereas bond failure was shown to occur in the specimens without the CFRP anchorage.

For a structure with excessive displacement from a continuous load over a long period or a structure requiring high flexural stiffness, it is difficult to provide adequate strengthening using just an FRP sheet or plate, as is the conventional practice. Moreover, there is a need

to supplement the greatest weakness of FRP, its brittleness. To solve this weakness of an FRP sheet or plate as a strengthening material, authors developed a composite beam that can simultaneously increase the flexural stiffness and flexural strength, as well as secure the ductility, of an RC structure. This composite beam, as shown in Figure 1, has a composite structure consisting of a hollow sectional aluminum core wrapped with GFRP (glass fiber-reinforced polymer). In our study, we produced specimens strengthened with this composite beam and specimens without such strengthening and experimentally assessed the improvement in load-carrying capacity and the load-displacement behavior of the beam. In addition, we proposed an analysis model to predict the behavior of a structure strengthened with the composite beam.

EXPERIMENTAL PROGRAM

Specimen design

Figure 2 shows a detailed specimen diagram and Table 1 summarizes the names of each specimen and variable. For this test, a total of 12 specimens, including 2 reference specimens, were prepared, each with an identical length of 4.4 m. The specimens were differentiated into two groups, Groups 1 and 2, based on their cross-sectional shape. Groups 1 and 2 had cross-sectional sizes of 600 × 200 mm (Figure 2a) and 300 × 450 mm (Figure 2b), respectively. For the Group 1 specimens, 5 steel bars of Φ13 mm were used to provide a 0.80% tensile reinforcement ratio, whereas the Group 2 specimens used 4 steel bars of Φ16 mm to provide a 0.65% tensile reinforcement ratio. In addition, Φ10 mm steel bars were used for the compressive reinforcement and shear reinforcement of all of the specimens and, in order to avoid the occurrence of shear failure prior to flexural failure, the shear reinforcing bars were placed at 100-mm intervals.

As test variables, the strengthening material type, epoxy type,

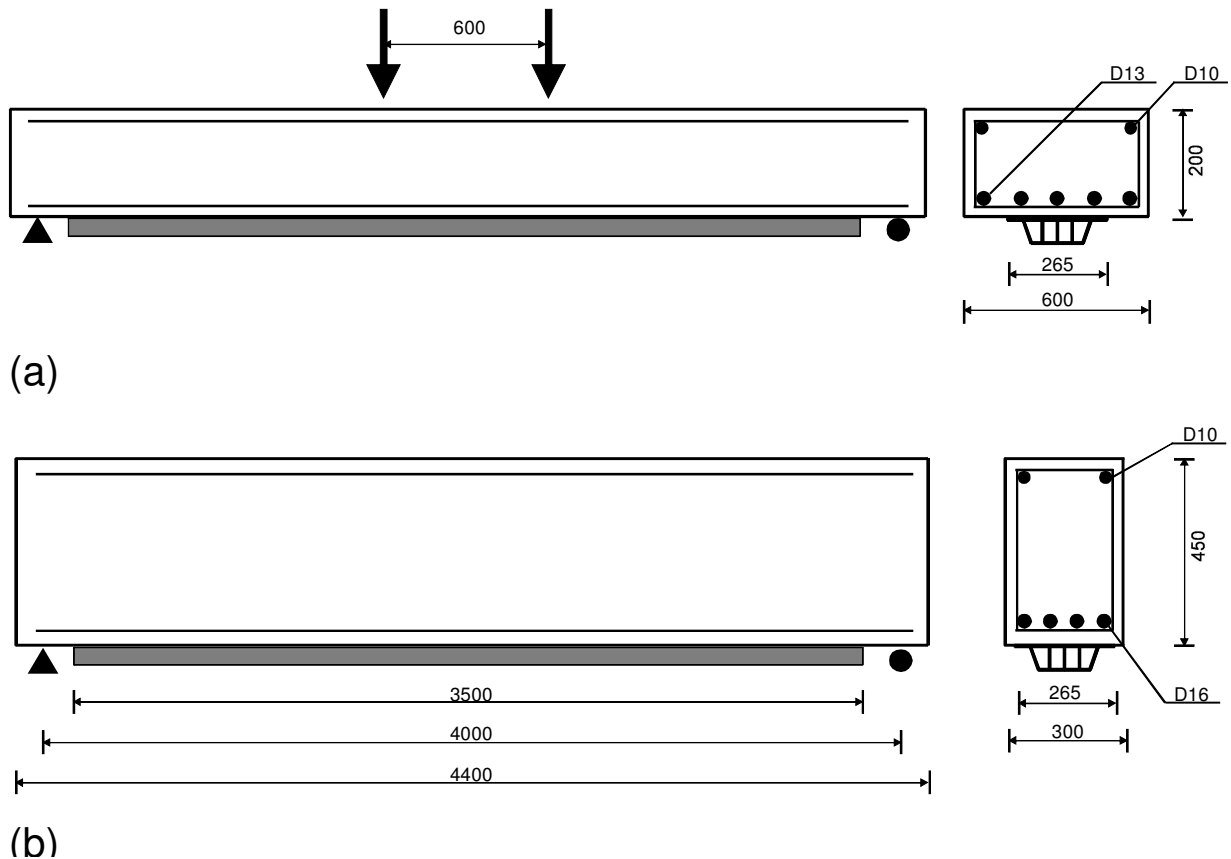


Figure 2. Test specimen geometry (dimension in mm): (a) Group 1, (b) Group 2.

Table 1. Specimen details and test variables.

Specimen	Section size $b \times h$ (mm)	Composite-beam type	Epoxy type	Power pin interval (mm)
S-U		-	-	-
S-AM1	600×200	Type-A	Ep-M	100
S-AE1		Type-A	Ep-E	100
S-AE2		Type-A	Ep-E	200
S-BE1		Type-B	Ep-E	100
S-BE2		Type-B	Ep-E	200
B-U			-	-
B-AM1	300×450	Type-A	Ep-M	100
B-AE1		Type-A	Ep-E	100
B-AE2		Type-A	Ep-E	200
B-BE1		Type-B	Ep-E	100
B-BE2		Type-B	Ep-E	200

S: 600 × 200 mm, B: 300 × 450 mm. U: Unstrengthened specimen. A: Type-A composite-beam, B: Type-B composite-beam. M: Ep-M, E: Ep-E. 1: Power pin interval 100 mm, 2: Power pin interval 200 mm.

and power pin interval were considered. Two composite beam types, as shown in Figure 3, were used as the strengthening materials. Each composite beam consisted of aluminum and GFRP, with the latter wrapped around the former. Type-A shown in Figure

3(a) had a width and height of 265 and 40 mm respectively, while Type-B shown in Figure 3(b) had a width and height of 260 and 12 mm respectively. A 3.5 m composite beam, taking up 87.5% of a specimen's net span, was used to strengthen the concrete tensile

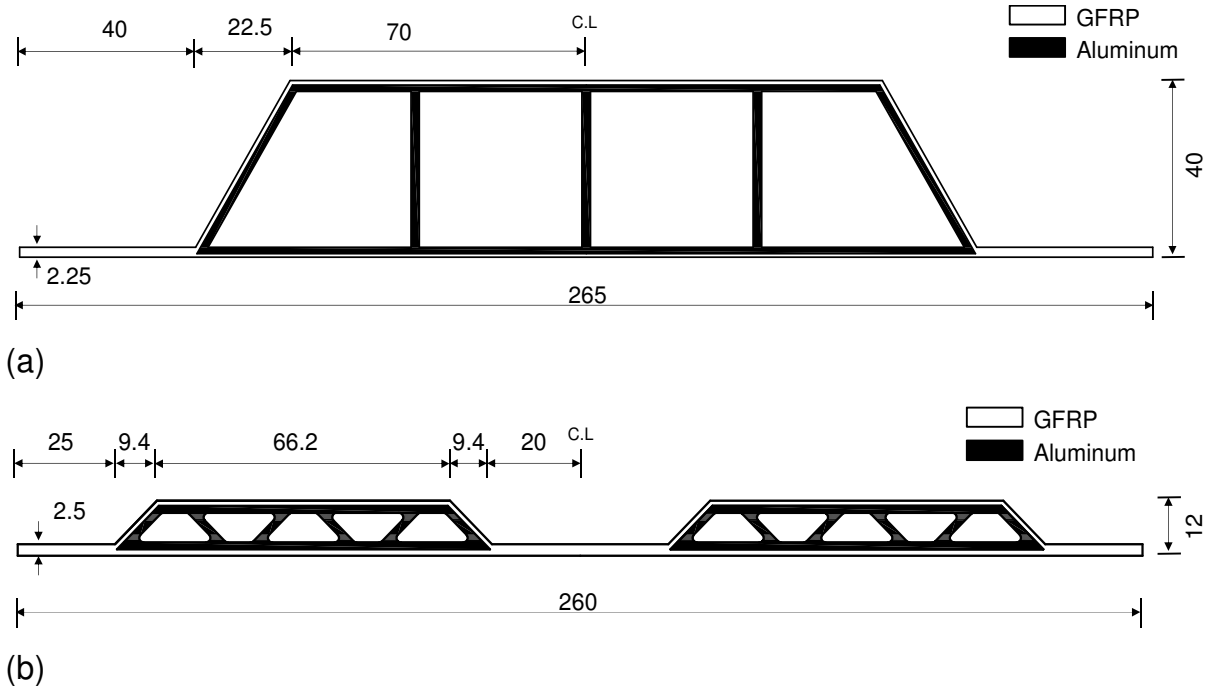


Figure 3. Composite-beam details (dimension in mm): (a) Type-A, (b) Type-B.

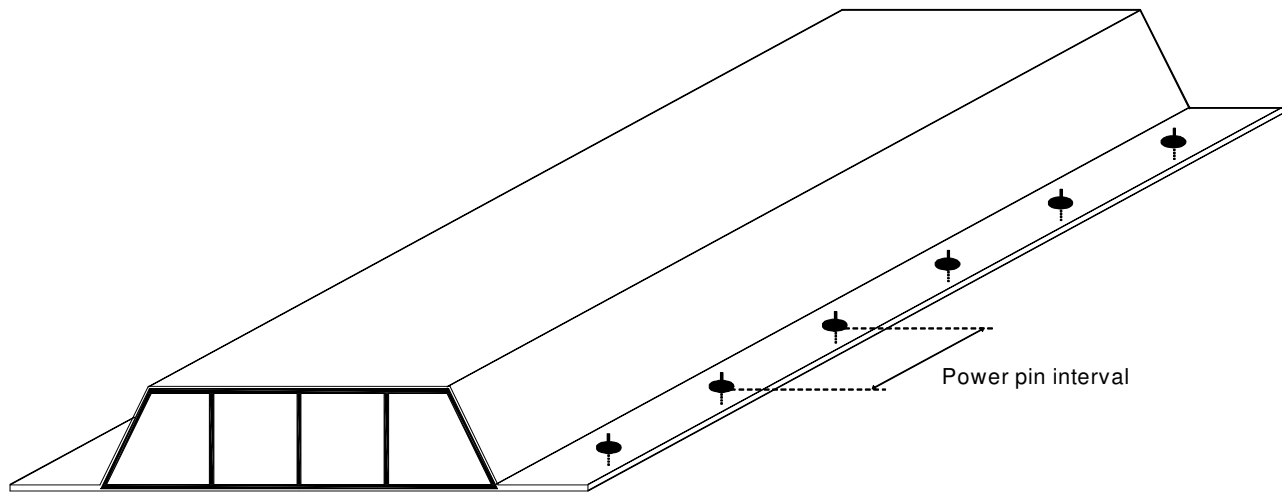


Figure 4. Power pin interval.

zone, as shown in Figure 2. Two types of epoxy, inorganic epoxy Ep-M and organic epoxy Ep-E, were used to bond the specimen and composite beam. The power pins served to hold the concrete and composite beam in place while the epoxy cured and, as shown in Figure 4, power pin intervals of 100 and 200 mm were chosen as test variables.

Materials

In this study, Type I Ordinary Portland cement and coarse aggregate with a maximum size of 25 mm were used in the

concrete mixture. Three $\Phi 100 \times 200$ mm cylinders were prepared at the same time that the specimen was cast and the 28 day compressive strength was measured. Table 2 shows the concrete mixture design used in this test. The compressive strength after 28 days was shown to be 21 MPa.

The composite beam used as the strengthening material was developed to improve the flexural stiffness and flexural strength of existing structures. As shown in Figure 3, each composite beam was a complex of aluminum and GFRP which were bonded at a high temperature. In order to have a correlation between Type-A and -B, they were designed to be composed of almost similar amounts of aluminum and GFRP. Table 3 shows the mechanical

Table 2. Concrete mixture design.

Design strength (MPa)	Slump (cm)	W/C (%)	S/a (%)	Unit weight (kg/m ³)				
				W	C	S	G	AE
21	12.0	53.2	51.3	163	306	913	901	1.53

Table 3. Mechanical properties of aluminum and GFRP.

Material	Tensile strength (MPa)	Ultimate tensile strain (%)	Modulus of elasticity (MPa)
Aluminum	235	6.27	71,500
GFRP	1100	1.07	103,000

Table 4. Mechanical properties of rebars.

Diameter (mm)	Yield strength (MPa)	Tensile strength (MPa)	Modulus of elasticity (MPa)
10	518	636	200,000
13	494	610	
16	506	608	

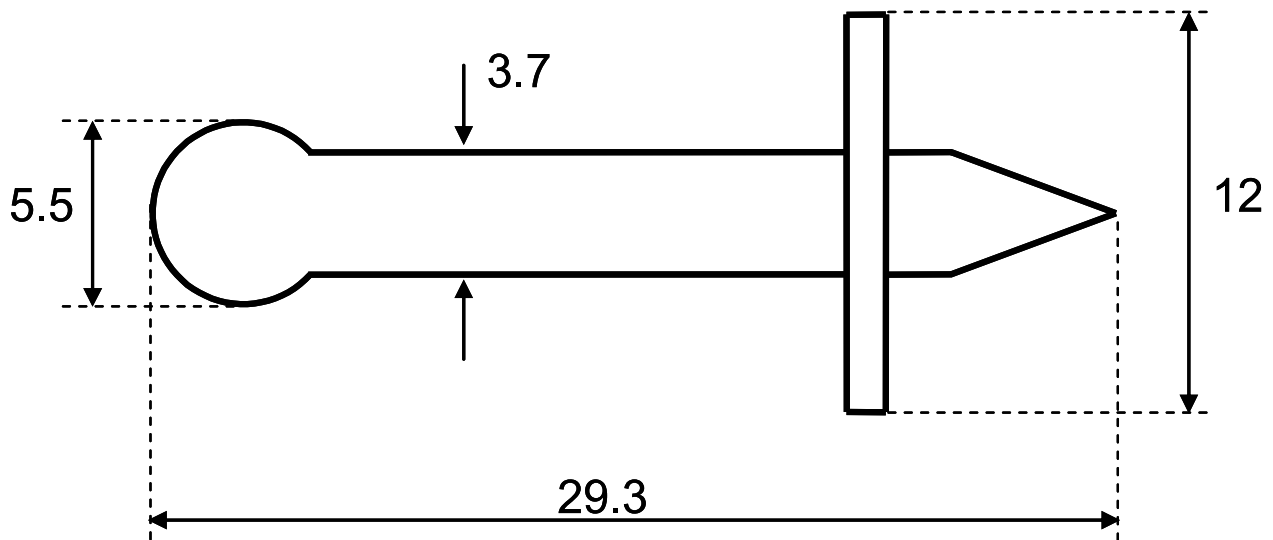


Figure 5. Power pin details (dimension in mm).

properties of the aluminum and GFRP used to produce the composite beams. The tensile reinforcements used in the specimen were $\Phi 13$ and $\Phi 16$ mm steel bars, while the compressive and shear reinforcements consisted of $\Phi 10$ mm steel bars. Table 4 shows the mechanical properties of the steel bars used in the specimen. The shear strengths of the epoxy Ep-M and Ep-E used in the composite beam bonding are respectively 15.1 and 11 N/mm². The shape of the power pin constructed to secure the bonding between the composite beam and concrete prior to the epoxy hardening is shown in Figure 5. A single power pin could bear a shear force of 400 N.

Specimen preparation

The specimen strengthening was done 28 days after the concrete was poured, in the following order, and this strengthening procedure is shown in Figure 6.

To improve the bonding efficiency, the tensile zone of the specimen was surface treated with a grinder, and the dust from the grinding was completely removed using an air compressor. Afterward, primer was applied to the surface to increase the adhesiveness between the concrete and composite beam. After mixing the main ingredients and the hardener of the epoxy resin

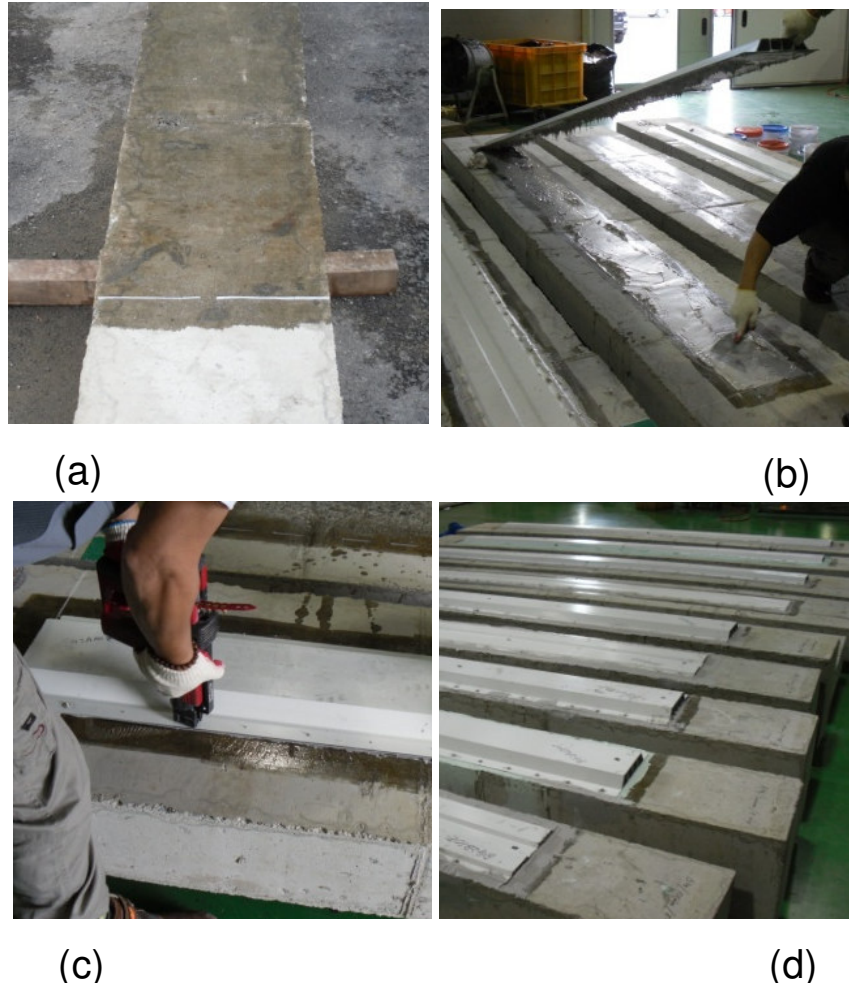


Figure 6. Order of specimen preparation: (a) Polymer application (b) Epoxy application (c) Composite beam bonding and power pin work, (d) Strengthening finish.

according to the prescribed mixing ratio, the mixture was applied to the tensile zone of the specimen and the composite beam was bonded. Before the epoxy hardened, power pins were installed to keep the composite beam and concrete from separating. This made it possible to fix the composite beam at the designated location and also increased the bonding efficiency of the composite beam and concrete. After all of the aforementioned work was performed, each specimen was cured for 7 days, and then the flexural test was performed.

Test method

Figure 7 shows the schematic diagram for loading system and measuring device. The loading was applied through the displacement control method at a rate of 0.02 mm/s until the point of specimen failure. To measure the displacement of the specimen center, 2 LVDTs (linear variable differential transformers) were installed at the center of the specimen. In addition, to observe the behavior of each material during the test, 2 strain gauges were attached at the center of the tensile reinforcement and 7 strain gauges were attached to the composite beam, as shown in Figure 7.

By using a data logger, all of the data were measured for each load phase until the test termination. In addition, the initial crack and crack progression in each specimen, as well as the failure and fracture of the composite beam, were visually observed and recorded, and the cracks occurring in each load phase were recorded on the surface of the concrete member. After the test termination, the specimen failure shape was photographed. The overall view of the test setup is shown in Figure 8.

TEST RESULTS AND DISCUSSION

The S-U and B-U specimens, as Groups 1 and 2 reference specimens, respectively, experienced flexural failures because of the yielding of the tensile reinforcement. The initial flexural crack occurred at the center of the load zone, and as the load increased, the crack width expanded. After the reinforcing bars yielded, the load did not increase, and when the displacement of the specimen increased greatly, concrete crushing began to occur.

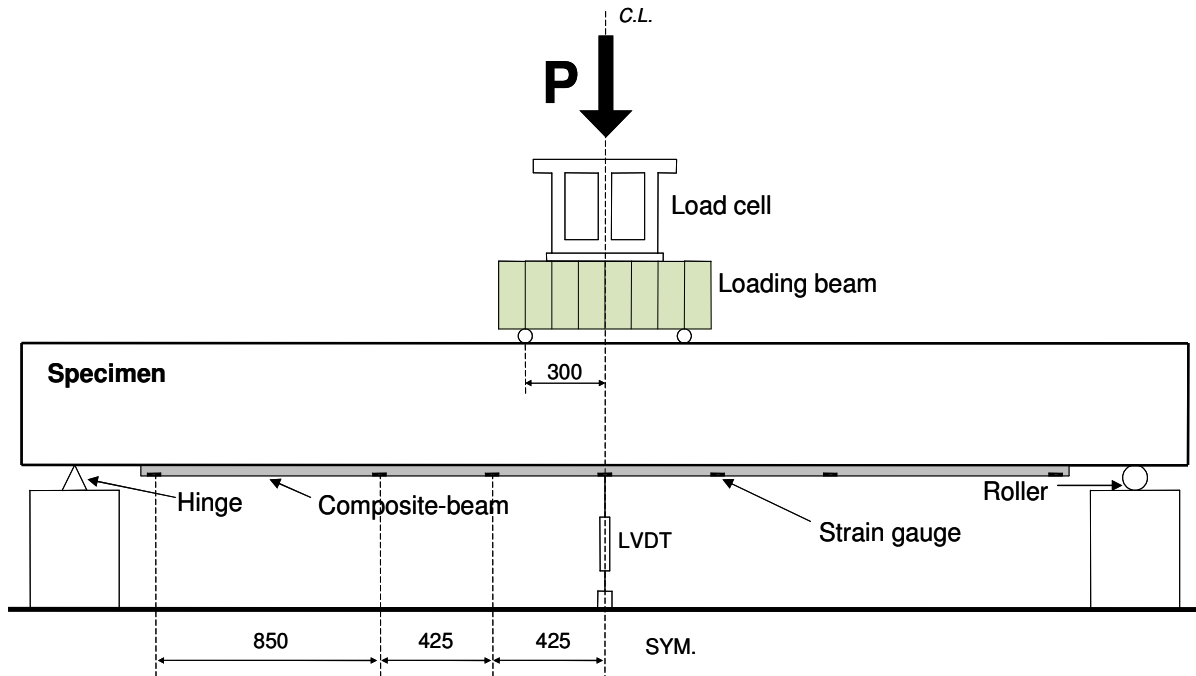


Figure 7. Schematic diagram for loading device and measuring system.

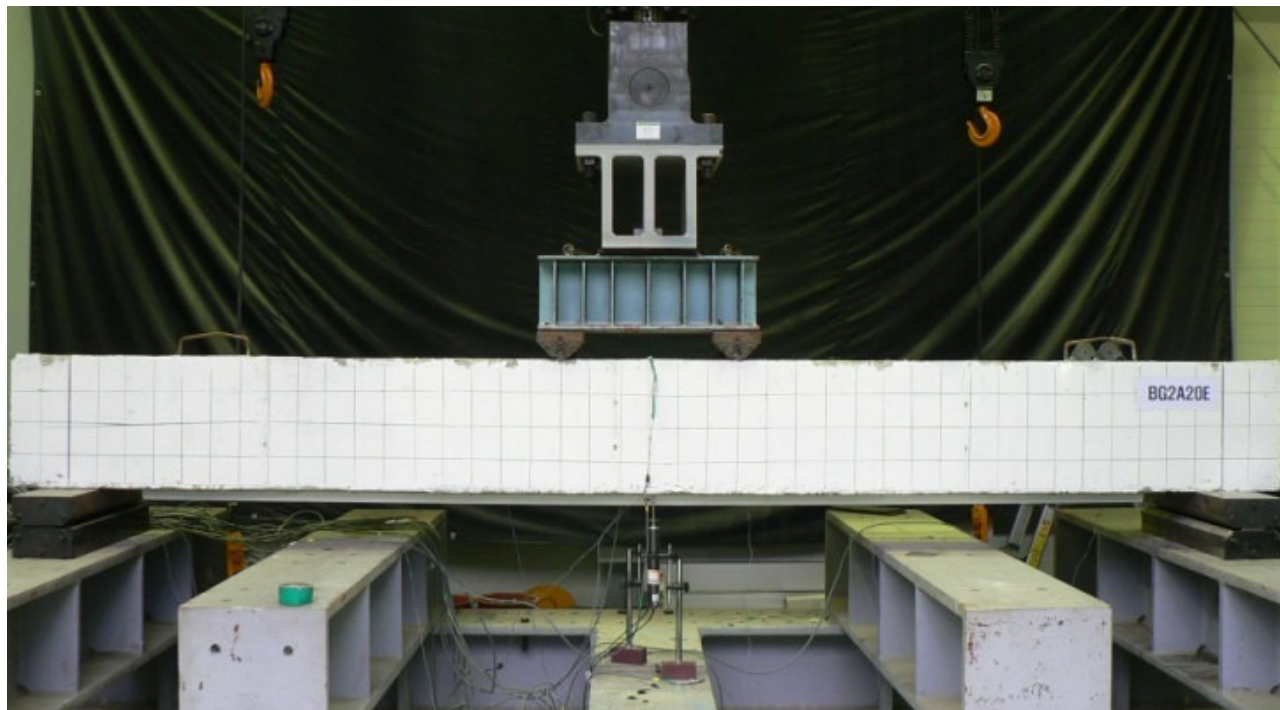


Figure 8. Overall view of test setup.

There were primarily two types of failure modes that happened to the composite beam-strengthened specimens. The first type was a bonding failure, which

consisted of the separation of the composite beam and concrete, as shown in Figure 9. This bonding failure began at the end of the composite beam and gradually



Figure 9. Debonding failure of composite-beam.



Figure 10. Fracture failure of composite-beam.

advanced to the center as the load increased. This initial separation of the composite beam occurred when the epoxy could not resist the shear stress created between the composite beam and concrete. Bonding failures happened to the S-AM1 and B-AM1 specimens, which used the Ep-M epoxy. The second failure type shown by the strengthened specimens was a composite beam fracture. Most of the specimens showed this failure mode, which could be considered the most effective failure

mode because it occurred after the bearing capacity of the composite beam was pushed to the maximum limit. When a load was applied to a specimen and it reached the maximum value, the composite beam underwent a rapid deformation. At that point, the aluminum, which has excellent ductility, responded flexibly to the load, but the brittle GFRP failed to respond and fractures occurred, as shown in Figure 10. These GFRP fractures occurred 2 to 3 times consecutively in the specimen's center, where the

Table 5. Results of tests.

Specimen	Initial cracking load (kN)	Yielding load (kN)	Maximum load (kN)	$\delta_{\text{maximum load}}$ (mm)	Rate of load increase (%)	Failure mode
S-U	11.6	42.0	51.6	110.0	-	FF [*]
S-AM1	12.8	63.8	68.3	61.7	32.4	DC ^{**}
S-AE1	13.1	95.0	95.0	39.8	86.2	FC ^{***}
S-AE2	12.9	90.3	90.3	34.5	75.6	FC
S-BE1	12.4	89.5	89.5	45.5	73.4	FC
S-BE2	18.1	93.2	93.2	22.8	80.6	FC
B-U	46.5	167.4	172.5	39.4	-	FF
B-AM1	53.6	202.3	202.3	11.6	17.3	DC
B-AE1	47.7	278.2	278.2	20.7	61.3	FC
B-AE2	47.1	271.7	271.7	25.6	57.5	FC
B-BE1	46.1	259.4	259.4	22.1	50.4	FC
B-BE2	45.5	230.0	251.9	23.9	46.0	FC

FF^{*}: Flexural failure. DC^{**}: Debonding of composite-beam. FC^{***}: Fracture of composite-beam.

flexural tensile force was the greatest, and most of the strengthened specimens showed ductile behavior after GFRP fracture of the composite beam. After the failure mode was set in the composite beam-strengthened specimens, the crushing of the compression zone concrete in all of the specimens began and the testing ended.

Table 5 shows the maximum load, load increase rate, and failure mode test results. The initial crack load was set based on the visually observed result and the load-displacement curve, and the reinforcing bar yield load was set based on strain measured with the strain gauges. Compared to non-strengthened reference specimens, all of the composite beam-strengthened specimens showed a large increase in flexural stiffness and maximum load. The strengthened specimens in Group 1 showed load increases of 32.4 to 86.2%, while the strengthened specimens in Group 2 showed increases of 17.3 to 61.3%.

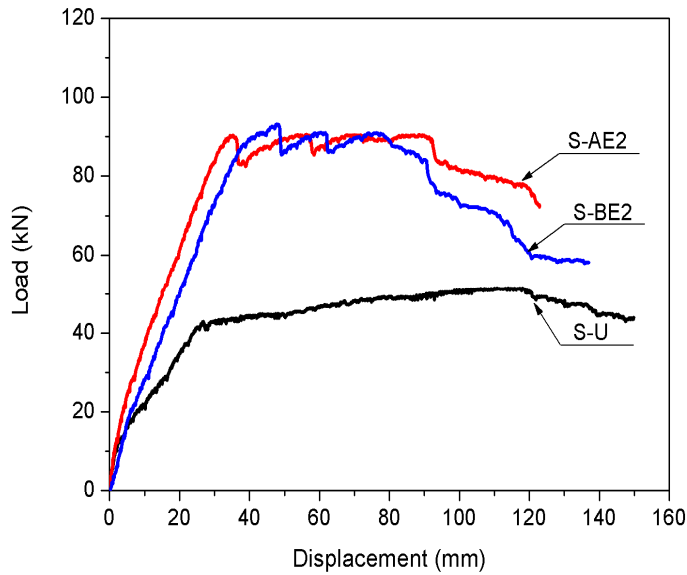
Impact of composite beam type

Figure 11 presents a comparison of the load-displacement curves with respect to the composite beam type. Figure 11(a) shows the load-displacement curves of the S-AE2 and S-BE2 specimens of Group 1, which had Type-A and -B composite beams, respectively, with identical Ep-E epoxy and power pin intervals of 200 mm. As seen in Figure 11(a), the S-AE2 specimen strengthened with the Type-A composite beam had a somewhat superior flexural stiffness than the S-BE2 specimen strengthened with the Type-B composite beam. It is hypothesized that the superior flexural stiffness manifested in the S-AE2 specimen was the result of the greater height of the Type-A composite beam compared

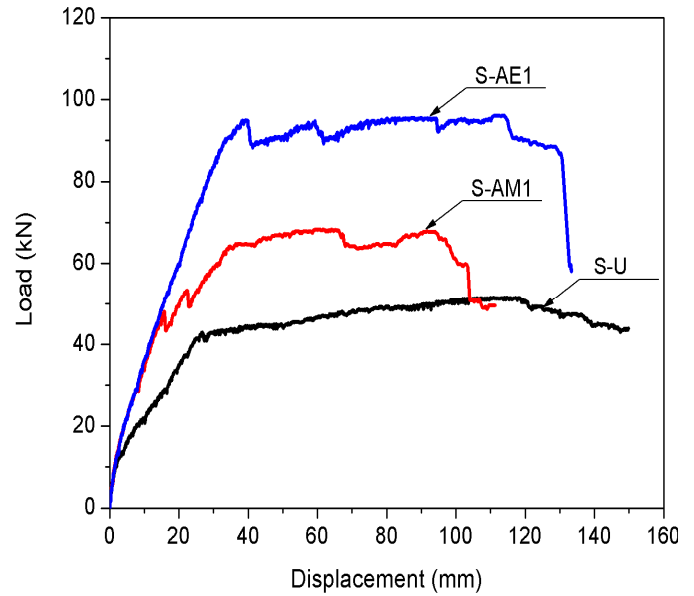
to the Type-B composite beam. However, it can also be verified from the figure that there is no significant difference between the load-displacement curves of the two specimens. Figure 11(b) shows the load-displacement curves of the B-AE2 and B-BE2 specimens of Group 2, which had Type-A and -B composite beams, respectively, with identical Ep-E epoxy and power pin intervals of 200 mm. Figure 11(b) shows that the flexural stiffness of the two specimens were almost the same. However, the maximum loads for the B-AE2 and B-BE2 specimens were 259.4 and 251.9 kN, respectively, showing the specimen strengthened with the Type-A composite beam had a somewhat greater maximum load. That is, it was confirmed that by using the Type-A composite beam, a larger flexural stiffness increase effect could be obtained for Group 1 specimens with a smaller effective depth, while a larger maximum load increase effect could be obtained for Group 2 specimens with a greater effective depth.

Impact of epoxy type

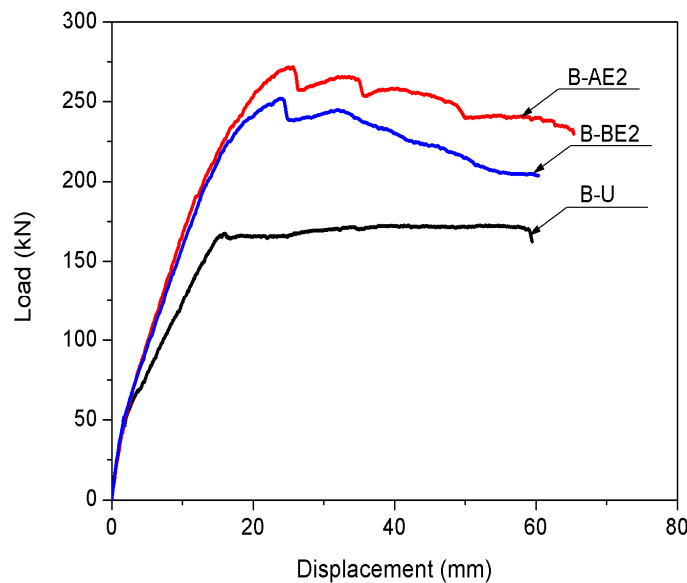
To assess the impact of the epoxy type, Figure 12 compares the load-displacement curves of the specimens strengthened using the Ep-A and Ep-B epoxies. S-AM1 and S-AE1, which are shown in Figure 12(a), were identically strengthened with Type-A composite beams and power pin intervals of 100 mm. The only difference between the two was the type of epoxy used, Ep-M or Ep-E. Figure 12(a) shows that for S-AM1, which used the Ep-M epoxy, bonding failure occurred in the concrete/composite beam interface before 100% of the material efficiency of the composite beam could be manifested. Compared to the maximum load of the reference specimen, S-U, the maximum loads of the S-AM1



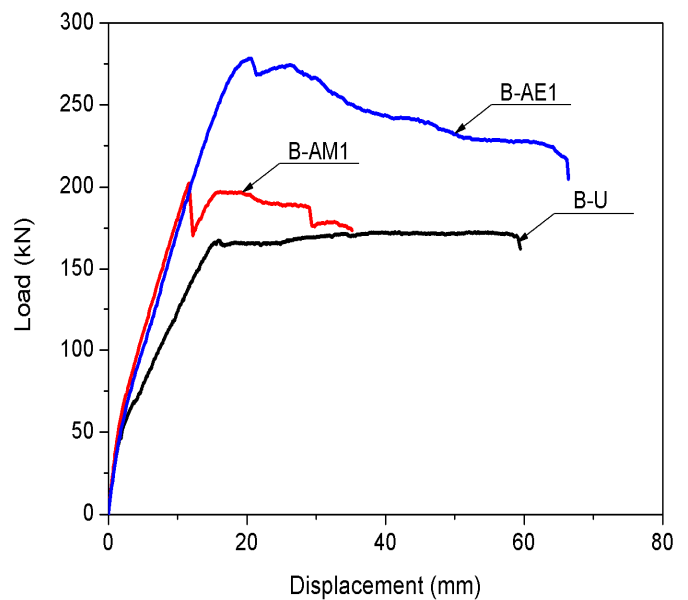
(a)



(a)



(b)



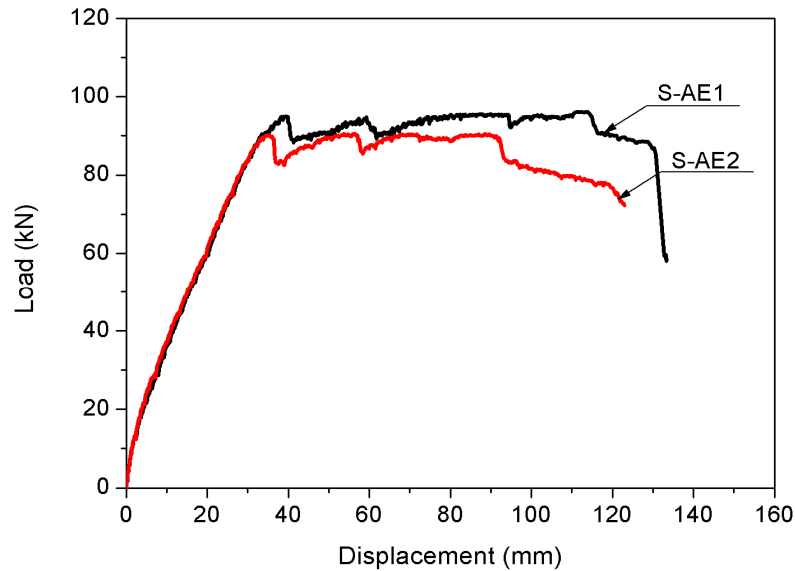
(b)

Figure 11. Comparison of load-displacement curves with respect to composite-beam type: (a) Group 1, (b) Group 2.

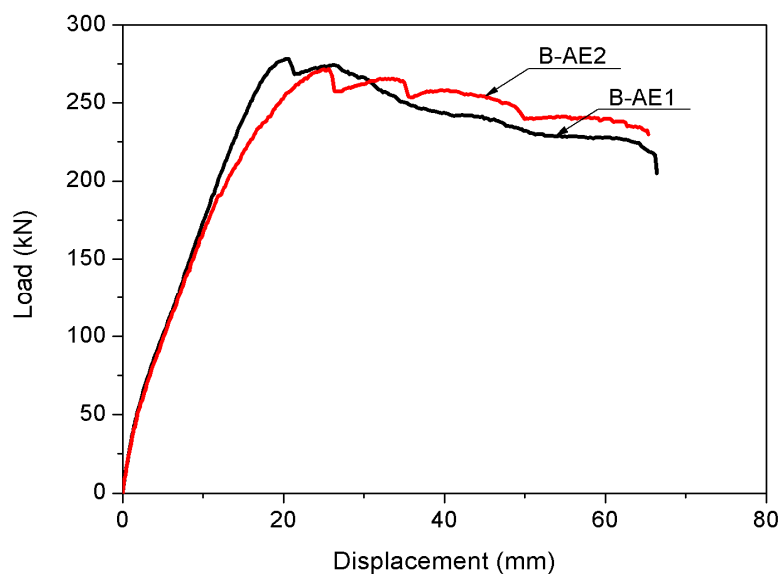
Figure 12. Comparison of load-displacement curves with respect to epoxy type: (a) Group 1, (b) Group 2.

and S-AE1 specimens increased by 32.4 and 86.2%, respectively, and there was a very large difference in the strengthening effects, depending on the epoxy type. Figure 12(b) shows the load-displacement curves of the Group 2 specimens that used identical Type-A composite beams and power pin intervals of 100 mm but different epoxy types, Ep-M and Ep-E. Figure 12(b) shows that for B-AE1, the specimen that used Ep-E epoxy, bonding failure did not occur until the material efficiency of the

composite beam was fully reached. In contrast, it did occur for the B-AM1 specimen, which used the Ep-M epoxy. Compared to the maximum load of the reference specimen, B-U, the maximum loads of the B-AM1 and B-AE1 specimens increased by 61.3 and 17.3%, respectively, and a clear difference between the strengthening effects was shown. Through this test, it was confirmed that the use of Ep-E epoxy could prevent the premature failure and secure an outstanding strengthening effect.



(a)



(b)

Figure 13. Comparison of load-displacement curves with respect to power pin interval: (a) Group 1, (b) Group 2.

Impact of power pin interval

Figure 13 shows the impact on the strengthening effect of the power pin used to fix the composite beam on the structure prior to epoxy hardening. Figure 13(a) shows the load-displacement curves of the S-AE1 and S-AE2 specimens, which used identical Type-A composite beams and Ep-E epoxy but different power pin intervals, 100 and 200 mm, respectively. Figure 13(a) shows that

the maximum load of the S-AE1 specimen was 5 kN greater than that of the S-AE2 specimen, but there was no significant difference in the load-displacement curves. Figure 13(b) shows the load-displacement curves of the B-AE1 and B-AE2 specimens from Group 2, which used identical Type-A composite beams and Ep-E epoxy but different power pin intervals, 100 and 200 mm, respectively. Figure 13(b) shows that the maximum load of the B-AE1 specimen with power pin intervals of 100

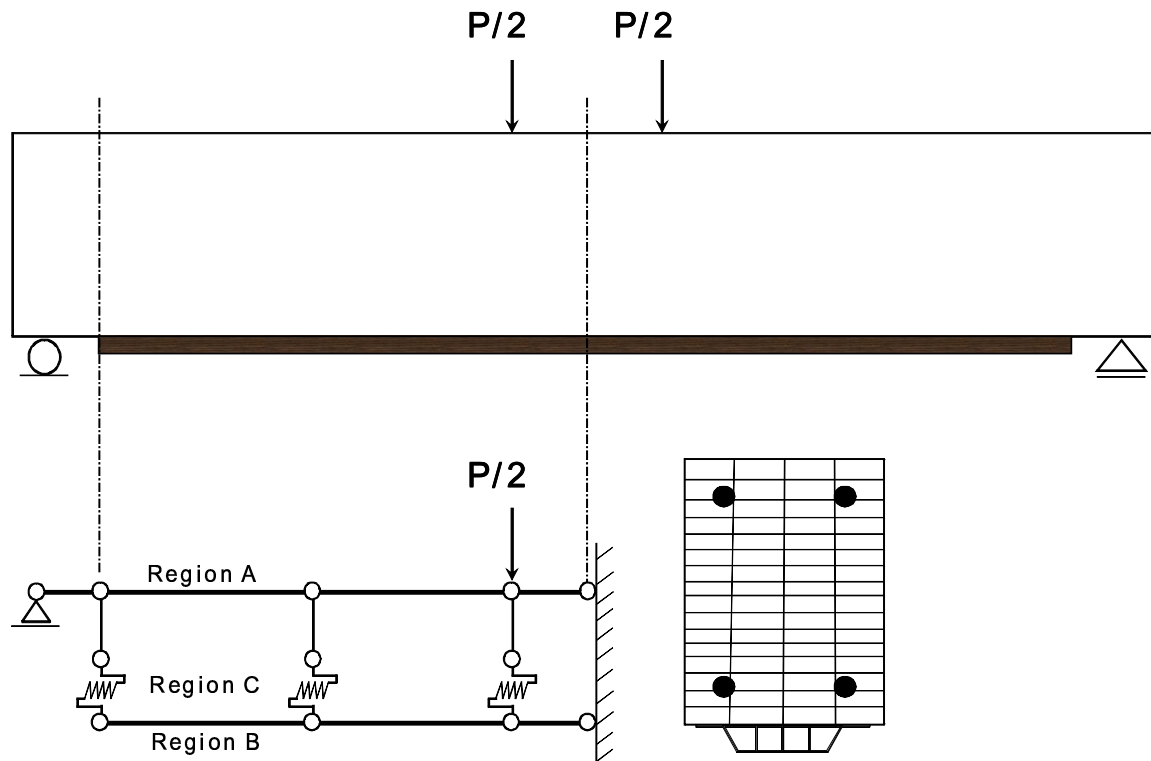


Figure 14. Proposed analysis model.

mm was 6 kN greater than that of the S-AE2 specimen with 200 mm intervals, but there was no significant difference in the load-displacement curves. Ultimately, from Figure 13, it can be seen that all of the specimens with 100 or 200 mm power pin intervals had adequate bonding strength.

FINITE ELEMENT ANALYSIS

Structural analysis model proposal

In this study, a finite element analysis model was proposed to analytically predict the composite behavior of RC beam strengthened with the composite beam. The analysis was performed by using the general structural analysis program OpenSees (2006). Figure 14 gives a schematic explanation of the proposed analysis model.

In this analysis model, 1/2 of a specimen is modeled to secure analytical speed and convergence. Because the number of elements connecting the nodal points was large, displacement-based, 2-dimensional beam-column elements were used. Region A in Figure 14 was constructed using fiber elements to idealize the steel concrete members. The height and width of the concrete cross-section were divided into 1/16 and 1/4 sized fiber elements, and the reinforcing bar was modeled by fiber with the cross-sectional size of the steel bar used in each

location. Region B was an element composed of a fiber cross-section to represent the composite beam. In Region B, the composite beam was modeled as a fiber cross-section composed of aluminum and GFRP. The proposed analysis model, unlike the existing model that defines the concrete and strengthening material as a single element, defines the concrete and strengthening material as separate elements. The concrete and composite beams were connected to a rigid beam element. The composite behavior of the concrete and composite beam was expressed through this rigid beam element. Region C was used to depict the bonding behavior of the concrete/composite beam interface. Region C was modeled using the ZeroLength element provided by OpenSees. In this study, the characteristics of the ZeroLength element used in Region C were utilized to define the bond-slip behavior between Region A and Region B. The nonlinear FE analyses are performed using an incremental displacement-controlled technique based on a Newton–Raphson iterative procedure in which the vertical displacement is applied at the loading points and the internal resisting force is computed. Here the displacement increment was set at 0.001 mm.

Material model

For the Region A concrete in Figure 14, the Concrete 02

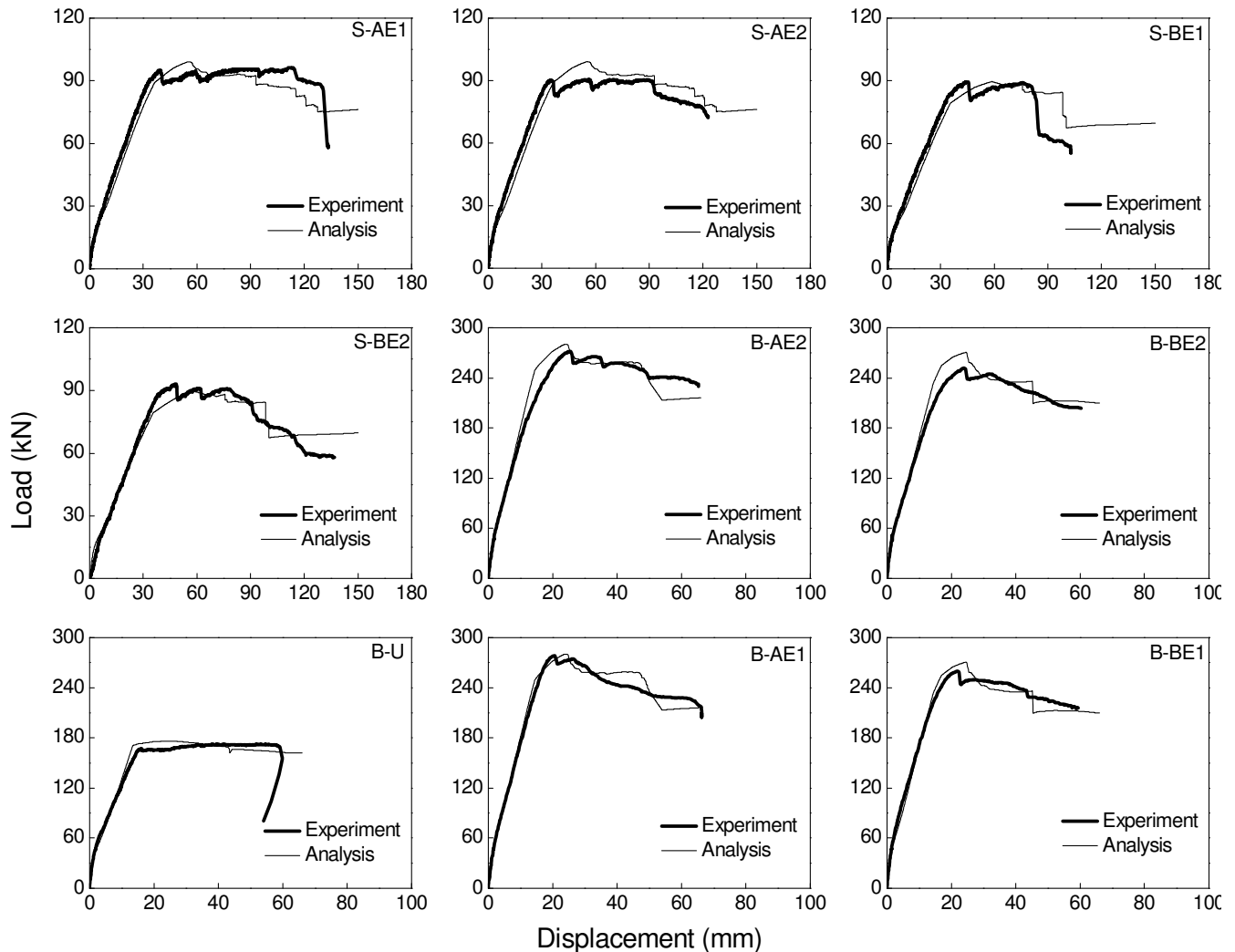


Figure 15. Comparison of test results and analysis results.

material model of OpenSees, which is based on the concrete model of Kent and Park (Kent and Park, 1971), was used to take the nonlinear characteristics into account. The Concrete 02 material model expresses the stress rising section and drop section of the compression zone as a parabola and straight line, respectively, with the stress rising section and drop section of the tensile zone expressed as straight lines. The bi-linear model was used as the material model of the reinforcing bar. The mechanical properties of the reinforcing bar were applied based on the material test results. Because the composite beam was composed of two materials, aluminum and GFRP, a different material model was used for each. For the aluminum material model, the same bi-linear model used for the reinforcing bar was used. The GFRP was modeled with the material judged to be brittle after the linear elastic section. To describe the bonding behavior of the concrete and composite beam, the bi-linear bond-slip model proposed by Lu et al.

(2005) was applied.

Comparison of test results and analysis results

Figure 15 compares the test results and analysis results from the application of the proposed analysis model. The analysis results for the Group 2 reference specimen, B-U, showed a somewhat large prediction value for the maximum load, but provided a relatively accurate prediction of the load-displacement behavior. In addition, the maximum load errors of the test and analysis results for the specimens strengthened with Type-A composite beams were found to be about 4 to 9%, while the values for the specimens strengthened with Type-B composite beams were 0 to 4%, showing very accurate maximum load predictions. Figure 15 also confirms that the analysis results provide relatively accurate predictions of the load-displacement behaviors of Groups 1 and 2 specimen in

both the elastic section and plastic section. Therefore, it is deemed that the analysis model proposed in this study could be very effectively utilized in predicting the flexural behavior of RC beam strengthened with the composite beam.

Conclusions

From the study on the flexural behavior characteristics of the composite beam- strengthened RC member, the following conclusions were drawn.

- (1) The stiffness and load increased in all of the specimens strengthened with the composite beam, compared to the reference specimens without such strengthening. The Groups 1 and 2 specimens respectively showed load increases of 32.4 to 86.2% and 17.3% to 61.3%.
- (2) It was verified that using the Type-A composite beam allowed a greater flexural stiffness increase effect to be obtained with a slender beam, while a greater load increase effect could be obtained with a deep beam. However, the difference was shown to be very slight.
- (3) For the strengthened specimens using the organic epoxy Ep-E, the tests terminated with the GFRP fracture of the composite beam, whereas for the strengthened specimens using the inorganic epoxy Ep-M, the tests terminated with the premature failure of the strengthening material. Hence, it was confirmed that using the Ep-E epoxy can prevent premature failure and provide an outstanding strengthening effect.
- (4) It is found that all of the specimens with 100 or 200 mm power pin intervals had adequate bonding strength.
- (5) Analysis results predicted with relative accuracy the load-displacement behaviors of the composite beam-

strengthened specimens in both the elastic and plastic sections. Therefore, it is deemed that the analysis model proposed in this study could be very effectively utilized in predicting the behavior of RC beam strengthened with the composite beam.

REFERENCES

- Chen JF, Teng JG (2001). Anchorage strength models for FRP and steel plates bonded to Concrete. *J. Struct. Eng., ASCE*, 127(7): 784-791.
- Ehsani MR, Saadatmanesh H, Tao S (1993). Bond of GFRP rebars to ordinary-strength concrete. *ACI Special Pub.*, (1): 333-345.
- Garden HN, Auantrill RJ, Hollaway LC, Thorne AM, Parke GAR (1997). An experimental study of the anchorage length of carbon fibre composite plates used to strengthen reinforced concrete beams. *Constr. Build. Mater.*, 12: 203-219.
- OpenSees (2006). <<http://opensees.berkeley.edu>>.
- Kent DC, Park R (1971). Flexural members with confined concrete. *J. Struct. Div. ASCE*, 97(ST7): 1969-1990.
- Lamanna AJ, Bank LC, Scott DW (2001). Flexural strengthening of RC beams using fasteners and FRP strips. *ACI Struct. J.*, 98(3): 368-376.
- Lu XZ, Tang JG, Ye LP, Jiang JJ (2005). Bond-slip models for FRP sheets/plates bonded to concrete. *Eng. Struct.*, 27: 920-937.
- El-Hacha R, H-Rizkalla S (2004). Near-surface-mounted fiber-reinforced polymer reinforcements for flexural strengthening of concrete structures. *ACI Struct. J.*, 101(5): 717-726.
- Seracino R, Raizal Saifulnaz MR, Oehlers DJ (2007). Generic debonding resistance of EB and NSM plate-to-concrete joints. *J. Comp. Construct.*, 11(1): 62-70.
- Teng, JG, Smith ST, Yao J, Chen JF (2003). Intermediate crack-induced debonding in RC beams and slabs. *Constr. Build. Mater.*, 17(6): 447-462.
- Woo SK, Nam JW, Kim JH, Han SH, Byun KJ (2008). Suggestion of flexural capacity evaluation and prediction of prestressed CFRP strengthened design. *Eng. Struct.*, 30: 3751-3763.
- Wu Z, Li W, Sakuma N (2006). Innovative externally bonded FRP/concrete hybrid flexural members. *Comp. Struct.*, 72: 289-300.